

Retention ratio and nonequilibrium bandspreading in asymmetrical flow field-flow fractionation

P. Stephen Williams¹

Received: 28 December 2014 / Revised: 16 April 2015 / Accepted: 22 April 2015 / Published online: 8 May 2015
© Springer-Verlag Berlin Heidelberg 2015

Abstract In asymmetrical flow field-flow fractionation (As-FIFFF), only the membrane-covered accumulation wall is permeable to fluid; the opposite channel wall is impermeable. Fluid enters the channel at the inlet and exits partly through the membrane-covered accumulation wall and partly through the channel outlet. This means that not only does the volumetric channel flow rate decrease along the channel length as fluid exits through the membrane but also the cross-channel component to fluid velocity must approach zero at the impermeable wall. This dependence of cross-channel fluid velocity on distance across the channel thickness influences the equilibrium concentration profile for the sample components introduced to the channel. The concentration profile departs from the exponential profile predicted for the ideal model of field-flow fractionation. This influences both the retention ratio and the principal contribution to bandspreading—the nonequilibrium contribution. The derivation of an equation for the nonequilibrium bandspreading parameter χ in As-FIFFF is presented, and its numerical solution graphed. At high retention, it is shown that the solutions for both retention ratio R and χ converge on those for the ideal model, as expected. At lower levels of retention, the departures from the ideal model are significant, particularly for bandspreading. For example, at a level of retention corresponding to a retention parameter λ of 0.05, R is almost 4 % higher than for the ideal model (0.28047 as compared to 0.27000) but the value of χ is almost 60 %

higher. The equations presented for both R and χ include a first-order correction for the finite size of the particles—the steric exclusion correction. These corrections are shown to be significant for particle sizes eluting well before steric inversion. For example, particles of half the inversion diameter are predicted to elute 25 % slower and to show almost 40 % higher bandspreading when steric effects are not accounted for. The work presented contributes to the fundamental theory of As-FIFFF and allows quantitative prediction of both retention and bandspreading at all levels of retention.

Keywords Asymmetrical flow field-flow fractionation · Isocratic operation · Retention ratio · Nonequilibrium bandspreading parameter

Introduction

Field-flow fractionation (FFF) is a separation and characterization technique for particles and macromolecules. It is similar in operation to liquid chromatography. A small sample is introduced into a fluid flowing through a thin channel rather than a chromatographic column, and sample components are differentially retained in the channel not by partition into a stationary phase but by the action of a field of some sort that is applied across the thickness of the channel. The sample particles or molecules, collectively referred to as particles hereafter, interact with the applied field and are driven across the channel thickness, away from the so-called depletion wall and toward the so-called accumulation wall. If the particles are sufficiently small (generally sub-micron), they quickly approach dynamic equilibrium distributions across the channel thickness where at every point transport toward the accumulation wall is exactly countered by diffusion away from the wall due to local concentration gradient. It is referred to as a dynamic equilibrium because

Published in the topical collection *Field- and Flow-based Separations* with guest editors Gaetane Lespes, Catia Contado, and Bruce Gale.

✉ P. Stephen Williams
p.stephen.williams@gmail.com

¹ Cambrian Technologies Inc., 1772 Saratoga Avenue, Cleveland, OH 44109, USA

particles are constantly moving by Brownian diffusion throughout the thickness of the concentration profile yet the concentration profile remains constant. For a field that is constant across the channel thickness, each component ideally attains a concentration profile that decays exponentially away from the accumulation wall, the mean thickness of which is equal to the ratio of the diffusion coefficient to the field-induced transport velocity across the channel thickness. Due to the no-slip condition at the channel walls and viscous drag, the fluid flowing along the channel has a parabolic velocity profile across the channel thickness, with zero velocity at the accumulation and depletion walls and maximum velocity at the channel center. The different sample components are separated as a result of their differing concentration distributions within this parabolic fluid velocity profile. Sample particles that are confined to thin layers close to the accumulation wall are carried by relatively slowly moving fluid, while particles forming thicker layers spend some of their time in faster moving fluid streams as well as those slower streams close to the wall. The fast exchange of particle positions within each concentration profile results in the migration of each component along the channel as a coherent band. The finite time for diffusion within each profile under the imposed shear flow does lead to a slight departure from equilibrium which gives rise to the primary contribution to bandspreading known as nonequilibrium bandspreading [1, 2].

The mechanism described above involving sub-micron materials is known as the normal mode of elution, as it corresponds to the original mode of operation envisioned for FFF [3]. It is also sometimes known as the Brownian mode due to the contribution of Brownian diffusion to the mechanism. A great advantage of this mode is that, in the ideal case, particle retention times and nonequilibrium bandspreading may be predicted from FFF theory. Conversely, particle properties may be derived from measurement of retention times without resort to calibration. It is this mode of FFF with which we are concerned here.

Many different fields have been utilized for FFF including gravitational [4], centrifugal [5–7], thermal gradient [8, 9], electrical [10, 11], and magnetic [12, 13]. Any field that interacts with a sample material property to drive the particles across the channel thickness may be used. There is a type of FFF that does not require a specific interaction with an applied field, however. In this type of FFF, the particles are carried across the channel thickness by a secondary, transverse component to fluid flow. It is consequently known as flow FFF, or FIFFF. In its original form [14], the two major walls of the channel are permeable. In addition to the fluid flow along the length of the channel, there is a secondary flow of fluid in through one of the walls and out through the other. This secondary flow carries the particles across the channel thickness simply by entrainment. The particles are retained in the channel by laying a semi-permeable membrane over the wall through which only the fluid then passes out of the channel. The membrane-covered porous wall serves as the

accumulation wall. Sub-micron particles approach differing transverse concentration distributions across the channel thickness only because of their differing diffusion coefficients. Smaller particles, having higher diffusion coefficients, form thicker, more diffuse layers next to the membrane and are eluted from the channel more quickly than larger particles. The proper setup for this form of FIFFF requires the flow rate through the depletion wall to equal the flow rate through the accumulation wall. The flow rate at the channel inlet will then necessarily equal the channel outlet flow rate. Ideally, the flux through each of the walls should also be uniform, which is more easily achieved for the membrane-covered accumulation wall than for the more porous depletion wall [15]. This form of FIFFF is known as symmetrical FIFFF (referred to here as Sym-FIFFF) due to the equalized transverse and longitudinal channel flow rates and assumed uniform wall flux.

A different form of FIFFF was introduced independently by Granger et al. [16] and by Wahlund and Giddings [17]. In this form of FIFFF, only the accumulation wall is permeable and the fluid flow at the channel outlet and through the membrane originates at the channel inlet. It follows that the volumetric flow rate decreases along the length of the channel. The system has certain similarities to hollow fiber FFF in that the elution flow and permeate flow originate at the inlet [18–22]. This form of FIFFF was named asymmetrical FIFFF (As-FIFFF, also sometimes referred to as AF⁴ or AF4) because of its characteristic flow setup, and it is this form of FIFFF with which we are concerned here. As-FIFFF has the advantage of eliminating potential problems associated with non-uniform flux through the depletion wall. However, for a channel of constant breadth, the mean flow velocity along the channel length necessarily decreases from the inlet to the outlet as fluid is lost through the accumulation wall. This can lead to problems in particle elution due to non-ideal effects such as those due to particle interactions with the membrane surface. These interactions tend to increase as flow velocity decreases, and consequently, some of the more retained particles may not elute. The decrease in mean flow velocity due to loss of volumetric flow rate along the channel length may be compensated by gradually reducing the channel breadth along its length. In 1991, Wahlund and Litzén [23] introduced the trapezoidal channel in which the channel breadth decreases linearly along its length. While the mean channel flow velocity in such a channel will not be constant, its variation can be greatly reduced in comparison to a channel of constant breadth. This arrangement has since become widely adopted. In 1997, a channel having an exponentially decreasing breadth was proposed for use in As-FIFFF. Such a channel not only has the benefits of the trapezoidal channel but also has the potential for isocratic operation with constant mean flow velocity along the channel length [24]. (We use the term isocratic, meaning equal power or strength, to indicate operation at constant cross flow rate.) This would be very useful for the study of

hydrodynamic lift forces in the steric mode of FIFFF [25, 26] where the variation of channel flow velocity would greatly complicate the interpretation of results. Note that the steric mode of FIFFF is more commonly referred to as lift-hyperlayer FIFFF due to the fact that the lift forces tend to drive particles relatively far from the accumulation wall. Particles of a given size are carried along the channel as a thin layer some distance from the accumulation wall; this layer being referred to as a hyperlayer [26]. It has been shown that constant channel flow velocity can also be advantageous for particle analysis in the normal mode [27]. This is because, as mentioned above, particle-membrane interactions increase as channel flow velocity is reduced, and particles may not elute if the flow velocity falls below some threshold. A varying channel flow velocity will carry particles not only through regions of the channel where the velocity is higher than the mean but also through regions where it is lower. These regions of lower flow velocity may be areas where particles are more likely to interact with the membrane and where they may even be adsorbed. It is therefore better to maintain a constant flow velocity so that there are no such regions of slower flow.

As-FIFFF is today the most widely used form of FFF, yet its theoretical description is incomplete. Retention and nonequilibrium bandspreading are commonly assumed to differ insignificantly from predictions based on the Sym-FIFFF model which is in turn assumed to correspond to the ideal model. While the theory for retention ratio (without the steric exclusion correction) has been presented before [17], and the small differences in comparison to the Sym-FIFFF are known, this is not the case for nonequilibrium bandspreading. The theory for nonequilibrium bandspreading in As-FIFFF is derived here for the first time, and this finally allows comparison of the two systems. It was expected that the results converge at high retention, but without the result of this derivation, it was not possible to predict the level of retention where they diverge significantly.

Assumptions regarding fluid flow and particle migration

It is assumed that the flux through the membrane over the accumulation wall is uniform. This requires that the pressure drop along the channel length be small compared to the pressure drop across the thickness of the membrane and the supporting porous frit, not only at the channel inlet but also at the channel outlet. The local mean fluid velocity along the channel length is also assumed to be uniform across the channel breadth and equal to the local channel volumetric flow rate divided by the local cross-sectional area of the channel. Except for the regions close to the side walls, this assumption will be reasonably good along the main body of the channel provided the channel thickness is uniform and the cross-

sectional aspect ratio of the channel is high. The assumption is less good in the region of the inlet and outlet endpieces where the flow from the inlet and toward the outlet has a radial pattern [28]. With the usual method of sample introduction and focusing used in As-FIFFF, the flow pattern in the inlet endpiece has little influence on the sample migration and bandspreading.

In addition, particle migration along the channel is assumed to be unperturbed by any non-ideal effects due to particle-wall and particle-particle interactions. Particles are assumed to migrate along the channel length at velocities equal to that of undisturbed fluid at the cross-channel positions of their centers. This assumption is not strictly valid when a particle is very close to a bounding wall [29–31], but for a diffuse layer of particles, in which there is a constant exchange of positions, particles will spend very little time next to the wall and the assumption is likely to be acceptable. The assumption becomes more valid as α decreases relative to λ . This effect is discussed in a little more detail in a later section.

The so-called steric exclusion effect is taken into account. This accounts for the fact that the center of a spherical particle cannot approach to within the particle radius of either the membrane or the upper wall [32, 33]. The spherical particle assumption is made for the purpose of deriving expressions for R and χ . In the later discussion of the significance of the steric correction, it is explained that the correction may be valid for non-spherical particles provided their aspect ratio is not too high.

The fluid velocity profile across the channel thickness is assumed to be parabolic in both Sym-FIFFF and As-FIFFF. This requires a no-slip boundary condition at the membrane surface and also at the upper permeable wall in Sym-FIFFF. This is an acceptable assumption for a typical ultrafiltration membrane but there may well be a small slip velocity for a porous frit wall [34]. The distortion of axial velocity profile due to cross flow in Sym-FIFFF would be negligible for the typical cross flow velocities employed [35]. This is also true for typical conditions used in As-FIFFF [16, 36].

Particle migration and nonequilibrium bandspreading are assumed to be described by the steady state mechanism corresponding to ideal FFF theory. This means that the transition from the initial focused zone to a migrating zone is not taken into account. Given the small transport distances across the zone thickness, this transition can be expected to occur very quickly following the start of migration.

The retention ratio

The retention ratio R is defined for a monodisperse collection of particles as the ratio of the mean local velocity of the

particles along the channel length to the mean local channel flow velocity, and is given by the equation

$$R = \frac{\langle c(x)v(x) \rangle}{\langle c(x) \rangle \langle v(x) \rangle} = \frac{\left(\frac{1}{w} \int_0^w c(x)v(x) dx \right)}{\left(\frac{1}{w} \int_0^w c(x) dx \right) \left(\frac{1}{w} \int_0^w v(x) dx \right)} \quad (1)$$

in which $c(x)$ and $v(x)$ are the concentration and channel flow velocity profiles as functions of the distance x across the channel thickness, measured from the accumulation wall, and w is the channel thickness. The angle brackets in Eq. (1) indicate the mean value of the enclosed functions across the channel thickness, as apparent from the final form on the right-hand side of Eq. (1).

The concentration profile across the channel thickness is obtained by considering the motion of particles toward the membrane caused by their entrainment in fluid exiting through the membrane and the diffusion away from the membrane according to Fick's first law of diffusion. The net flux of particles away from the membrane J_x is given by

$$J_x = -|u|c - D \frac{dc}{dx} \quad (2)$$

where u is the local fluid velocity across the channel thickness in the x -direction, c is the local particle concentration, and D is the particle translational diffusion coefficient. Note that u is generally negative, and its absolute value is included in Eq. (2), consistent with the FFF literature. At steady state, the flux becomes zero at all x , and it can then be seen that

$$\int_{c_0}^c \frac{dc}{c} = - \int_a^x \frac{|u|}{D} dx \quad (3)$$

in which c_0 is the particle concentration at the point of closest approach of a particle center to the membrane surface (corresponding to particle radius a in the case of a spherical particle).

In As-FIFFF, the cross flow fluid velocity is not constant across the channel thickness. It falls to zero at the impermeable depletion wall. The cross flow velocity as a function of x is given by [17]

$$|u| = |u_0| \left(1 - \frac{3x^2}{w^2} + \frac{2x^3}{w^3} \right) \quad (4)$$

where $|u_0|$ is the cross flow velocity at the membrane surface, given by

$$|u_0| = \frac{\dot{V}_c}{A_C} = \frac{\dot{V}_c w}{V_C^0} \quad (5)$$

where \dot{V}_c is the cross-channel volumetric flow rate exiting through the membrane, A_C is the area of the membrane-covered accumulation wall, and V_C^0 is the volume of the channel.

Substitution of Eq. (4) into Eq. (3) results in the concentration profile given by

$$c(x) = c_0 \exp \left(-\frac{x}{\ell_0} \left(1 - \frac{x^2}{w^2} + \frac{x^3}{2w^3} \right) + \frac{a}{\ell_0} \left(1 - \frac{a^2}{w^2} + \frac{a^3}{2w^3} \right) \right) \quad (6)$$

in which $\ell_0 = D/|u_0|$. We can now let $\zeta = x/\ell_0$ and $\lambda_0 = \ell_0/w$, so that $x/w = \lambda_0 \zeta$. The concentration profile for $\alpha/\lambda_0 \leq \zeta \leq (1-\alpha)/\lambda_0$ may then be given in the form

$$\begin{aligned} c(\zeta) &= c_0' \exp(-\zeta(1-\lambda_0^2 \zeta^2 + 0.5\lambda_0^3 \zeta^3)) \\ &= c_0' \exp(-f(\zeta)) \end{aligned} \quad (7)$$

where c_0' is the concentration extrapolated to $x=0$:

$$c_0' = c_0 \exp \left(\frac{\alpha}{\lambda_0} (1-\alpha^2 + 0.5\alpha^3) \right) \quad (8)$$

and the function $f(\zeta)$ is defined by

$$f(\zeta) = \zeta(1-\lambda_0^2 \zeta^2 + 0.5\lambda_0^3 \zeta^3) \quad (9)$$

The parabolic fluid velocity profile across the channel thickness is given by

$$v(x) = 6\langle v \rangle \frac{x}{w} \left(1 - \frac{x}{w} \right) \quad (10)$$

which may then be written in the form

$$v(\zeta) = 6\langle v \rangle \lambda_0 \zeta (1-\lambda_0 \zeta) \quad (11)$$

Substituting Eqs. (7) and (11) into Eq. (1) and excluding the regions of steric exclusion from the integrals, we obtain the following expression for the steric-corrected retention ratio in As-FIFFF:

$$R = \frac{6\lambda_0 \int_{(1-\alpha)/\lambda_0}^{\alpha/\lambda_0} \zeta(1-\lambda_0 \zeta) \exp(-f(\zeta)) d\zeta}{\int_{\alpha/\lambda_0}^{(1-\alpha)/\lambda_0} \exp(-f(\xi)) d\xi} \quad (12)$$

This expression differs from that previously published [17] by including a first-order correction for finite particle size through the limits of the integrals. The retention ratio with

steric exclusion correction for the ideal model of FFF and assumed to describe retention in Sym-FIFFF is given by [32]

$$R = 6\alpha(1-\alpha) + 6\lambda \left((1-2\alpha)\coth\left(\frac{1-2\alpha}{2\lambda}\right) - 2\lambda \right) \quad (13)$$

in which $\lambda = \mathcal{A}w = D/|u|w$, and $|u|$ is assumed to be constant across w . The hyperbolic cotangent rapidly approaches unity as λ decreases (for example, $\coth(3.0) = 1.0049698$ and $\coth(5.0) = 1.0000908$). Equation (13) may therefore be approximated by [37]

$$R = 6\alpha(1-\alpha) + 6\lambda(1-2\alpha-2\lambda) \quad (14)$$

which is accurate to within 0.5 % for $\lambda \leq 0.15$ and $\alpha \leq 0.05$.

The concentration profile in As-FIFFF, described by Eq. (7), deviates slightly from the exponential profile found in Sym-FIFFF. For a given \dot{V}_c/A_C , the concentration decays a little more slowly in the asymmetrical case because the fluid cross flow velocity component decreases with distance from the accumulation wall. For a given \dot{V}_c/A_C , the value of λ_0 for As-FIFFF will be equal to the λ for Sym-FIFFF, but the retention ratio will be greater for As-FIFFF than for the symmetrical case.

Figure 1 shows plots of R as a function of λ_0 from 0 to 0.25 for both As-FIFFF and Sym-FIFFF (R_{As} and R_{Sym} , respectively). Numerical methods were used for solution of the integrals in Eq. (12). Note that λ_0 for Sym-FIFFF is defined as for As-FIFFF in terms of cross-channel fluid velocity component at the membrane, remembering that ideally this is constant across the channel thickness. The range of λ_0 chosen for the R -plots is sufficient to compare retention ratios up to around 0.8. Elution at higher retention ratios is not useful for determining sample properties or for significant separation. In the interests of clarity, the steric correction is not included (α is set to zero). Steric correction could have been included in one of two ways, neither of which is particularly helpful or appealing. Either an arbitrary constant value for α could be considered (the figure then representing the result of varying cross flow rate for a fixed particle size) or α could vary inversely with λ_0 around some arbitrary value (the figure then representing the retention ratios for a range of particle sizes at fixed cross flow rate). The inclusion of an equivalent steric contribution to both R_{Sym} and R_{As} would simply reduce their relative difference a little. It is far better to make the comparison with omission of the steric correction. This is not to say that the correction is unimportant as explained later. Also shown in Fig. 1 is a plot of the ratio of the two functions, R_{As}/R_{Sym} . It is seen that $R_{As} > R_{Sym}$ for $0 < \lambda_0 \leq 0.25$. In fact, R_{Sym} just exceeds R_{As} for λ_0 greater than around 0.5, but this is of only academic interest at this level of retention. The difference is greatest (just over 11 %) at λ_0 of 0.12, but less than 4 % at λ_0 of 0.05 where $R_{Sym} = 0.27000$ and $R_{As} =$

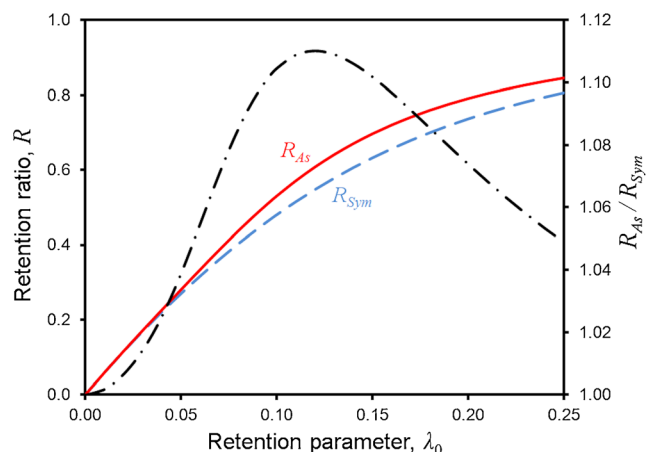


Fig. 1 Retention ratio for As-FIFFF (R_{As} , full red curve) and for Sym-FIFFF (R_{Sym} , dashed blue curve) as functions of retention parameter λ_0 . Ratio of the retention ratios (dot-dashed black curve) plotted against the right-hand axis

0.28047. As λ_0 becomes smaller, the particles are confined to thinner regions close to the membrane where the flow conditions in As-FIFFF more closely match those of Sym-FIFFF, and the difference in R becomes smaller.

Nonequilibrium bandspreading

As mentioned earlier, the nonequilibrium contribution to bandspreading is generally the major contribution to bandspreading in FFF. We expect the nonequilibrium contribution to bandspreading to be larger in the case of As-FIFFF as compared to Sym-FIFFF (for given \dot{V}_c/A_C) because of the slower decay of concentration away from the accumulation wall. We also expect the bandspreading of As-FIFFF and Sym-FIFFF to converge as retention increases and particles are confined to a thin region close to the membrane.

Giddings [1] showed how the departure from equilibrium concentration distribution caused by the shear flow of the carrier fluid could be described in terms of an equilibrium departure function $\varepsilon(x)$ defined by

$$c(x) = c^*(x)(1 + \varepsilon(x)) \quad (15)$$

where $c(x)$ is the actual concentration profile and $c^*(x)$ is the equilibrium concentration profile which corresponds to the profile expected when it is not disturbed by the shear flow. The equilibrium profile $c^*(x)$ therefore corresponds to Eq. (6) for As-FIFFF. Effective separation requires that $\varepsilon(x)$ be small over most of the system so that elution takes place in near-equilibrium conditions. He showed that, by consideration of the transport equations in the cross-channel and longitudinal directions, a second-order differential equation in ε could be derived. Following this approach, we obtain

$$D \frac{\partial^2 \varepsilon}{\partial x^2} - |u(x)| \frac{\partial \varepsilon}{\partial x} = (v(x) - R \langle v \rangle) \frac{\partial \ln c^*}{\partial z} \quad (16)$$

where z is the distance along the channel length. Note that in Eq. (16), we include the functional dependence of cross-channel velocity u on position x , and a negative sign appears on the left-hand side of the equation because the absolute value of u is considered. The variation of u across the channel thickness was not considered in the previous derivations of nonequilibrium bandspreading. Equation (16) may be converted to dimensionless variables by substituting a new dimensionless nonequilibrium function ϕ for the dimensionless function ε , where they are related by

$$\phi = \frac{\varepsilon D}{R \langle v \rangle \ell_0^2 \partial \ln c^* / \partial z} \quad (17)$$

The transverse distance x is converted to dimensionless ζ defined previously as $\zeta = x/\ell_0$, and the local fluid velocity is reduced by the zone velocity,

$$\mu(\zeta) = \frac{v(\zeta)}{R \langle v \rangle} = \frac{6\lambda_0 \zeta (1 - \lambda_0 \zeta)}{R} \quad (18)$$

Equation (16) can then be transformed to the following:

$$\frac{d^2 \phi}{d\zeta^2} - (1 - 3\lambda_0^2 \zeta^2 + 2\lambda_0^3 \zeta^3) \frac{d\phi}{d\zeta} = \mu(\zeta) - 1 \quad (19)$$

In the original derivation [1, 2], no account was taken of steric exclusion, and it was required that Eq. (19) be solved for $\phi(\zeta)$ subject to the boundary condition $d\phi/d\zeta = 0$ at the accumulation wall and the condition $\langle c^* \phi \rangle = 0$.

The contribution to nonequilibrium bandspreading is given by the equation [1, 2]:

$$H = \chi w^2 \langle v \rangle / D \quad (20)$$

where χ is the nonequilibrium bandspreading parameter given by

$$\chi = -2\lambda_0^2 R \langle c^* \Phi (\mu - 1) \rangle / \langle c^* \rangle \quad (21)$$

in which c^* , Φ , and μ are all functions of position across the channel thickness, and $\Phi = \phi - g_1$ where g_1 is the value of ϕ at $\zeta = 0$ (consistent with the condition $\langle c^* \phi \rangle = 0$). The relationship between Φ and ϕ means that Φ can be obtained directly by solution of the differential equation

$$\frac{d^2 \Phi}{d\zeta^2} - (1 - 3\lambda_0^2 \zeta^2 + 2\lambda_0^3 \zeta^3) \frac{d\Phi}{d\zeta} = \mu(\zeta) - 1 \quad (22)$$

with boundary conditions $\Phi = 0$ and $d\Phi/d\zeta = 0$ at $\zeta = 0$ when steric exclusion is not considered. We can include the

consideration of steric exclusion by solving Eq. (22) with the boundary conditions $\Phi = 0$ and $d\Phi/d\zeta = 0$ at $\zeta = \alpha/\lambda_0$, and the result can be written in the form

$$\Phi(\zeta) = \int_{\alpha/\lambda_0}^{\zeta} \exp(f(\zeta)) \int_{\alpha/\lambda_0}^{\zeta} \exp(-f(\zeta)) (\mu(\zeta) - 1) d\zeta d\zeta \quad (23)$$

with $f(\zeta)$ defined by Eq. (9). The value of χ is obtained by solving Eq. (21) which may be written in the form

$$\chi = -2\lambda_0^2 R \frac{\int_{\alpha/\lambda_0}^{(1-\alpha)/\lambda_0} \exp(-f(\zeta)) \Phi(\zeta) (\mu(\zeta) - 1) d\zeta}{\int_{\alpha/\lambda_0}^{(1-\alpha)/\lambda_0} \exp(-f(\zeta)) d\zeta} \quad (24)$$

with $\mu(\zeta)$ given by Eq. (18), R given by Eq. (12), and $\Phi(\zeta)$ given by Eq. (23).

We note that the determination of χ does not, in fact, require that Φ equal zero at $\zeta = \alpha/\lambda_0$. This is because

$$\int_{\alpha/\lambda_0}^{(1-\alpha)/\lambda_0} \exp(-f(\zeta)) (\mu(\zeta) - 1) d\zeta = 0 \quad (25)$$

which may be shown to be true by rearrangement of Eq. (12). Therefore, any non-zero value for Φ at $\zeta = \alpha/\lambda_0$ (which would simply be a constant added to Eq. (23)) would have no net contribution to the integral in the numerator of Eq. (24). Only one boundary condition is therefore required for solution of Eq. (22), that being $d\Phi/d\zeta = 0$ at $\zeta = \alpha/\lambda_0$. An arbitrary constant of integration would then be included in Eq. (23). We set $\Phi(\alpha/\lambda_0) = 0$ only for convenience.

The numerical evaluation of Eq. (24) is computationally non-trivial since the numerator contains three levels of integration. The equation may be simplified in the same manner used for the derivation of the symmetrical case [2], taking into account Eq. (25), reducing the numerator to two levels of integration. After rearrangement, the result for the product χR may be written as

$$\chi R = 2\lambda_0^2 \frac{\int_{\alpha/\lambda_0}^{(1-\alpha)/\lambda_0} \exp(f(\zeta)) \left[\int_{\alpha/\lambda_0}^{\zeta} \exp(-f(\zeta)) (6\lambda_0 \zeta (1 - \lambda_0 \zeta) - R) d\zeta \right]^2 d\zeta}{\int_{\alpha/\lambda_0}^{(1-\alpha)/\lambda_0} \exp(-f(\zeta)) d\zeta} \quad (26)$$

The reduction of levels of integration from three to two results in a considerable saving in numerical computation.

We also note that integration of the numerators of Eqs. (24) or (26) are to be carried out over the interval from α/λ_0 to $(1-\alpha)/\lambda_0$. The upper limit $(1-\alpha)/\lambda_0$ increases with decrease of λ_0 , with the result that for small λ_0 integration would be carried out over regions where there should be negligible contribution to the result. This would be a waste of computational effort, but, more importantly, rounding errors in the lower level integrals in these regions can lead to catastrophic error in the final result. In practice, using a Digital Visual Fortran compiler (Version 5.0, Digital Equipment Corporation, 1997) with double precision, it was found that results were stable and accurate if the integration was restricted to the interval from α/λ_0 to $(\alpha+25\lambda_0)/\lambda_0$ for $\lambda_0 < (1-2\alpha)/25$.

For Sym-FIFFF, the product of χ and R with inclusion of the simple steric exclusion correction is given by [32, 33, 37]

$$\chi R = 12 \lambda^2 \left[\left\{ 336\lambda^4 + 24(1-2\alpha)^2\lambda^2 - (1-2\alpha)^4 \right\} - \left\{ 120(1-2\alpha)\lambda^3 - 6(1-2\alpha)^3\lambda \right\} \coth\left(\frac{1-2\alpha}{2\lambda}\right) - \left\{ 12(1-2\alpha)^2\lambda^2 - (1-2\alpha)^4 \right\} \coth^2\left(\frac{1-2\alpha}{2\lambda}\right) - 6(1-2\alpha)^3\lambda \coth^3\left(\frac{1-2\alpha}{2\lambda}\right) \right] \quad (27)$$

which reduces for conditions where $\coth((1-2\alpha)/2\lambda) \rightarrow 1$ to

$$\chi R = 144\lambda^4 \left[(1-2\alpha)^2 - 10(1-2\alpha)\lambda + 28\lambda^2 \right] \quad (28)$$

Dividing Eq. (28) by Eq. (14) gives the following approximate expression for χ :

$$\chi = \frac{24\lambda^4 \left[(1-2\alpha)^2 - 10(1-2\alpha)\lambda + 28\lambda^2 \right]}{\alpha(1-\alpha) + \lambda(1-2\alpha-2\lambda)} \quad (29)$$

which for negligible α reduces to

$$\chi = \frac{24\lambda^3(1-10\lambda+28\lambda^2)}{(1-2\lambda)} \quad (30)$$

Figure 2 shows plots of χ as a function of λ_0 , again for the relevant range of λ_0 from 0 to 0.25, for the two forms of FIFFF (χ_{As} and χ_{Sym} , respectively). The steric exclusion correction was omitted in the interest of clarity for the same reasons given for the comparison of retention ratios. The χ parameter is larger for As-FIFFF than for Sym-FIFFF for λ_0 up to about 0.23. Also shown is the plot of the ratio of χ_{As}/χ_{Sym} . The magnitude of χ_{As} is more than twice that of χ_{Sym} for λ_0 between about 0.075 and 0.095 (corresponding to R between

around 0.38 and 0.5), but the difference decreases for higher levels of retention. At $\lambda_0=0.05$ (corresponding to $R_{As}=0.28047$), $\chi_{Sym}=0.0019000$, whereas $\chi_{As}=0.0030255$ which is almost 60 % higher. At $\lambda_0=0.025$ (corresponding to $R_{As}=0.14393$), $\chi_{Sym}=0.00030296$ and $\chi_{As}=0.00033845$ and the difference is less than 12 %. At $\lambda_0=0.02$ ($R_{As}=0.11595$), $\chi_{Sym}=0.00016224$ and $\chi_{As}=0.00017420$; a difference of less than 7.4 %.

Nonequilibrium plate height for isocratic elution

Consider the channel to be divided into small, discrete intervals along its length. There will be a contribution to bandspreading within each interval. To take into account the falling volumetric flow rate along the channel length and the variation in channel breadth, the contributions to variance in zone breadth on the channel are not simply added. The variance at the previous interval is adjusted for the change in mean fluid velocity before the contribution to variance at the current interval is added. For this consideration of isocratic elution, we need only consider that $\langle v \rangle$ is some function of z . We indicate this dependence on discrete positions z_i using the notation $\langle v(z_i) \rangle$, and the velocity-adjusted summation may then be written as

$$\sigma_i^2 = \sum_{j=1}^i c \delta \sigma_j^2 = \delta \sigma_i^2 + \left(\frac{\langle v(z_i) \rangle}{\langle v(z_{i-1}) \rangle} \right)^2 \sum_{j=1}^{i-1} c \delta \sigma_j^2 \quad (31)$$

where the subscript C on the summation sign indicates that it does not represent a simple summation—it is a velocity-corrected summation. The result σ_i^2 is the velocity-corrected sum of the contributions to variance for intervals 1 to i . The mean fluid velocity is a function of distance along the channel. The dependence on distance in turn depends on the volumetric flow rates at the channel inlet and outlet (together determining the flow rate through the membrane) and on the variation of channel breadth along the channel. Expanding the final term in the summation on the right-hand side of Eq. (31) shows that

$$\sum_{j=1}^i c \delta \sigma_j^2 = \delta \sigma_i^2 + \left(\frac{\langle v(z_i) \rangle}{\langle v(z_{i-1}) \rangle} \right)^2 \left\{ \delta \sigma_{i-1}^2 + \left(\frac{\langle v(z_{i-1}) \rangle}{\langle v(z_{i-2}) \rangle} \right)^2 \sum_{j=1}^{i-2} c \delta \sigma_j^2 \right\} \quad (32)$$

and therefore

$$\sum_{j=1}^i c \delta \sigma_j^2 = \delta \sigma_i^2 + \left(\frac{\langle v(z_i) \rangle}{\langle v(z_{i-1}) \rangle} \right)^2 \delta \sigma_{i-1}^2 + \left(\frac{\langle v(z_i) \rangle}{\langle v(z_{i-2}) \rangle} \right)^2 \sum_{j=1}^{i-2} c \delta \sigma_j^2 \quad (33)$$

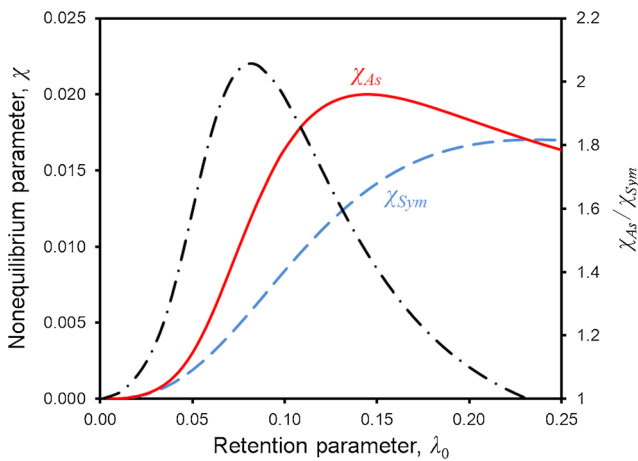


Fig. 2 Nonequilibrium parameter for As-FIFFF (χ_{As} , full red curve) and for Sym-FIFFF (χ_{Sym} , dashed blue curve) as functions of retention parameter λ_0 . Ratio of the parameters (dot-dashed black curve) plotted against the right-hand axis

Successive expansions show that for isocratic operation

$$\begin{aligned}\sigma_i^2 &= \sum_{j=1}^i c \delta\sigma_j^2 = \sum_{j=1}^i \left(\frac{\langle v(z_i) \rangle}{\langle v(z_j) \rangle} \right)^2 \delta\sigma_j^2 \\ &= \langle v(z_i) \rangle^2 \sum_{j=1}^i \frac{\delta\sigma_j^2}{\langle v(z_j) \rangle^2}\end{aligned}\quad (34)$$

The absence of the subscript C on the summation signs in the two right-hand formulae indicates that these represent simple summations. Rearranging Eq. (34) and dividing through-out by the square of the local zone velocity ($=R\langle v(z_i) \rangle$) shows that for the case of isocratic elution, the result reduces to a simple summation of contributions to variance in elution time $\delta\sigma_{ij}^2$:

$$\sigma_{ii}^2 = \frac{\sigma_i^2}{(R\langle v(z_i) \rangle)^2} = \sum_{j=1}^i \frac{\delta\sigma_j^2}{(R\langle v(z_j) \rangle)^2} = \sum_{j=1}^i \delta\sigma_{ij}^2 \quad (35)$$

where σ_{ii}^2 is the resulting variance in elution time at interval i . This is equivalent to the situation in gas chromatography where local gas velocity varies due to its compressibility [38]. In the case of programmed cross flow rate in As-FIFFF, the variance in elution time does not reduce to the simple summation of Eq. (35), however.

The local nonequilibrium plate height at position z_j along the channel is given by [2]

$$H_{\text{neq}}(z_j) = \frac{\chi w^2}{D} \langle v(z_j) \rangle \quad (36)$$

where the nonequilibrium bandspreading parameter χ is a function of the retention parameter λ or λ_0 and ratio of particle

radius to channel thickness α .

For a small migration distance δz , the local contribution to variance of the zone breadth on the channel is given by

$$\delta\sigma_j^2 = H_{\text{neq}}(z_j) \delta z = \frac{\chi w^2}{D} \langle v(z_j) \rangle \delta z \quad (37)$$

The local zone velocity dz/dt is given by

$$\frac{dz}{dt} = R \langle v(z_j) \rangle \quad (38)$$

and therefore, substituting for δz in Eq. (37) using Eq. (38),

$$\delta\sigma_j^2 = \frac{\chi R w^2}{D} \langle v(z_j) \rangle^2 \delta t \quad (39)$$

Figure 3 shows plots of the product χR versus λ_0 for the two forms of FIFFF (given by Eqs. (26) and (27), respectively), as well as their ratio. The product χR is relevant to the local contribution to zone variance as shown by Eq. (39) above. Finally, Fig. 4 shows plots of $\chi R/144\lambda_0^4$ versus λ_0 for each case. Also included is a plot of the function $(1-10\lambda_0+28\lambda_0^2)$ which is consistent with the approximate Eq. (28) for Sym-FIFFF. This illustrates how good the approximation of Eq. (28) is for λ_0 up to around 0.15 in Sym-FIFFF. At $\lambda_0=0.15$ and $\alpha=0$, Eq. (28) overestimates χR_{Sym} by less than 5.8%. Unfortunately, such an accurate and simple approximation for χR_{As} is not available.

From Eqs. (34) and (39)

$$\sigma_i^2 = \sum_{j=1}^i c \delta\sigma_j^2 = \langle v(z_i) \rangle^2 \frac{\chi R w^2}{D} \sum_{j=1}^i \delta t \quad (40)$$

If it is assumed that retention time $t_r=(i+f)\delta t$ where $0 \leq f < 1$ (so that f is the final fraction of an interval in δt), and $z_{i+f}=L$, then the variance in zone breadth at the channel outlet is given by

$$\sigma^2 = \langle v_L \rangle^2 \frac{\chi R w^2}{D} t_r = \langle v_L \rangle^2 \frac{\chi w^2 t^0}{D} \quad (41)$$

where $\langle v_L \rangle$ is the mean flow velocity at the outlet, and t^0 is the void time, or non-retained time, for migration from the focusing point to the outlet, so that under isocratic conditions, $R=t^0/t_r$. The variance in retention time σ_r^2 is then given by dividing Eq. (41) by the square of zone velocity at the channel outlet:

$$\sigma_r^2 = \frac{\sigma^2}{(R\langle v_L \rangle)^2} = \frac{\chi w^2 t^0}{R^2 D} \quad (42)$$

which, for ideal elution behavior, is seen to be independent of the channel breadth profile. For isocratic elution, the apparent plate height contribution due to nonequilibrium bandspreading is given by

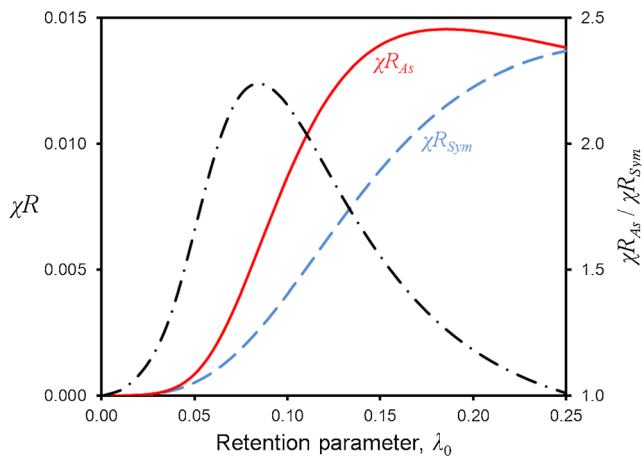


Fig. 3 Product of χR for As-FIFFF (χR_{As} , full red curve) and for Sym-FIFFF (χR_{Sym} , dashed blue curve) as functions of retention parameter λ_0 . Ratio of the products (dot-dashed black curve) plotted against the right-hand axis

$$\bar{H}_{neq} = (L-z') \frac{\sigma_t^2}{t_r^2} \quad (43)$$

where $L-z'$ is the elution path length from the focusing point z' to the channel outlet and σ_t^2 is given by Eq. (42). The retention time t_r is simply equal to t^0/R , so that

$$\bar{H}_{neq} = \frac{\chi w^2 (L-z')}{D t^0} = \frac{\chi w^2}{D} \langle \bar{v} \rangle \quad (44)$$

in which $\langle \bar{v} \rangle (= (L-z')/t^0)$ is the time averaged mean channel flow velocity along the elution path. The form of this equation for \bar{H}_{neq} is consistent with the result presented by Litzén and Wahlund [23], although we now have the correct solution for the steric-corrected χ for As-FIFFF. The apparent

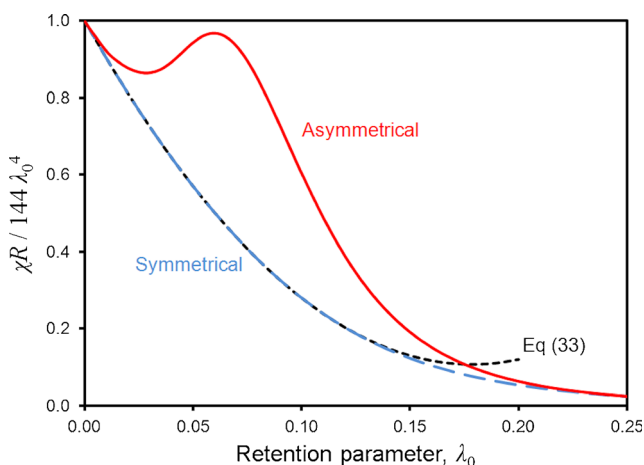


Fig. 4 The function $\chi R/144\lambda_0^4$ for As-FIFFF (full red curve) and for Sym-FIFFF (dashed blue curve) versus retention parameter λ_0 . Also included is the curve corresponding to $(1-10\lambda_0+28\lambda_0^2)$ consistent with the approximate Eq. (28) for Sym-FIFFF (dashed black curve)

nonequilibrium plate height is seen to be proportional to χ , and the ratio of plate height expected in Sym-FIFFF to that in As-FIFFF will therefore correspond to the χ_{As}/χ_{Sym} plot shown in Fig. 2.

It should be pointed out that this treatment of velocity-corrected summation of contributions to zone variance for a sample zone migrating along an As-FIFFF channel is not strictly correct. Except for the special case of the exponential channel with flow rates adjusted for constant mean fluid velocity along the channel, the system is non-uniform in both the local mean particle migration velocity and local plate height. Conditions therefore vary across the finite breadth of a migrating zone. For the approach described by Eqs. (31) to (44), it is assumed that the zone has a variance determined by conditions experienced by the center of mass as it migrates along the channel. This is the approach taken for the integral method of determining retention and bandspreading in forms of FFF where the channel flow velocity is uniform along the channel length (although it may vary with time) [37, 39–43]. Blumberg and Berger [44] have discussed zone migration in non-uniform systems. They showed that non-uniformity always gives rise to a loss of efficiency, but the effect was generally very small. We can therefore assume that the predictions of bandspreading based on Eqs. (31) to (44) will be acceptable.

Influence of steric correction on retention and nonequilibrium bandspreading

Extrapolation of Eq. (13) or Eq. (14) to very high field strength or cross flow where λ approaches zero puts retention into the steric mode. The limiting equation, $R=6\alpha(1-\alpha)$, corresponds to the simplistic model of steric FFF in which spherical particles move at a velocity equal to that of undisturbed fluid at a distance of one particle radius from the wall. Experiments showed that this model is not realistic; particles are driven away from the wall by hydrodynamic lift forces and are retarded relative to the fluid by other hydrodynamic effects [45]. An empirical correction factor γ , of order unity, was included in the simplistic equation to account for these effects. It was found that γ was a function of channel flow velocity, field strength or cross flow rate, and particle size. In studies of the steric inversion phenomenon, it was assumed that the γ function could be extrapolated from the steric mode through the inversion point [46]. It was subsequently included in the steric-corrected retention ratio equation for the normal mode which implied that there was some uncertainty associated with the steric correction. Of course, the inclusion of γ does not exclude the possibility that γ approaches unity in the range of normal mode elution. A theoretical modeling of the influence of hydrodynamic retardation of spherical particles close to the channel walls on the retention ratio in normal mode FFF

hydrodynamic chromatography has been carried out by Pasol et al. [31]. They did not include any tendency for particles to be driven away from the walls in this model. Values of λ of 0.01, 0.05, 0.1, 0.2, and ∞ (no field) were considered, and calculated R graphed over the complete range of α from 0 to 0.5. The calculated R converge on those predicted by Eq. (13) as α approaches zero, as expected, but the wide range of α makes it difficult to discern the difference between the solutions when $\alpha < \lambda \ll 1$, which is the region with which we are concerned here. Shendruk et al. [47] later presented experimental results supporting the model, but again, the experiments were not relevant to the typical range of steric-corrected normal mode FFF.

The best evidence for the validity of the simple steric correction for spherical particles comes from studies of the perturbation to retention ratios due to particle-wall interactions [48]. Equation (14) was modified to include an additional term δ_w to account for the interaction:

$$R = 6\alpha(1-\alpha) + 6\lambda(1-2\alpha-2\lambda)(1 + \delta_w/\ell) \quad (45)$$

in which $\ell = \lambda w$, and δ_w corresponds to a positive distance in the case of a repulsion. It was found that δ_w was independent of particle diameter d in sedimentation FFF when there was a significant repulsion (found when using a carrier solution of low ionic strength, for example). Moreover, when ionic strength of the carrier solution was sufficiently high and a good surfactant used, then δ_w was insignificant. The approach has also been applied to Sym-FIFFF, and δ_w was again seen to decrease with increase of ionic strength of the carrier solution [49]. These studies suggest that the simple steric exclusion model is valid for spherical particles when particle-wall repulsion can be suppressed. Perturbations due to other influences, such as lift forces, particle-wall interactions, sample overloading, etc., can be considered secondary effects.

Finally, it may be assumed that Eqs. (12) to (14) and (26) to (30) will be a reasonable approximation for particles that are not spherical but do not have a major axis that differs greatly from the others, i.e., particles that are not thin plates or long rods. Such particles close to the wall will tend to tumble over their major axis in the shear flow, and the value for α will be determined by the dimensions of the major axis. Different behavior may be expected for particles of high aspect ratio such as plate-like particles or long carbon nanotubes, for example, where rotation may be hindered [50–53]

The significance of the steric correction to both retention and nonequilibrium bandspreading can be deduced from the following. We suppose that Eqs. (12) and (13) are acceptably accurate for some range of α/λ , and consider the case of strong retention where $\lambda \ll 1$ and $\alpha \ll 1$. The retention ratio for both Sym-FIFFF and As-FIFFF is then given by

$$R = 6\alpha + 6\lambda \quad (46)$$

We can assume that Eq. (46) breaks down before steric inversion or not, but it is simple to show that for FIFFF where $\alpha \propto d$ and $\lambda \propto 1/d$, the projected steric inversion occurs at the point where $\alpha_i = \lambda_i$ (where the subscript i refers to the inversion point). For a particle that is some fraction f of the projected inversion diameter, but not so small that the $\lambda \ll 1$ condition breaks down, we see that

$$R = 6f\alpha_i + 6\lambda_i/f = 6\lambda_i(f + f^{-1}) \quad (47)$$

If retention time is normalized by the projected inversion time t_{ri} , we obtain

$$\frac{t_r}{t_{ri}} = \frac{12\lambda_i}{6\lambda_i(f + f^{-1})} = \frac{2}{(f + f^{-1})} \quad (48)$$

and if retention time predicted without the steric correction t'_r is normalized in the same way

$$\frac{t'_r}{t_{ri}} = \frac{12\lambda_i}{6\lambda_i/f} = 2f \quad (49)$$

Equations (48) and (49) are plotted in Fig. 5, labeled t_r , as the full blue line and red dashed line, respectively. They are seen to diverge well below the inversion diameter. For a particle just half the inversion diameter, the uncorrected t'_r is 25% higher than the corrected t_r ($t_r = 0.8 t'_r$). The error in calculated particle diameter caused by ignoring the steric correction would be 20% (this is indicated by the dashed black line that shows t'_r for $d=0.4 d_i$ is equal to t_r for $d=0.5 d_i$).

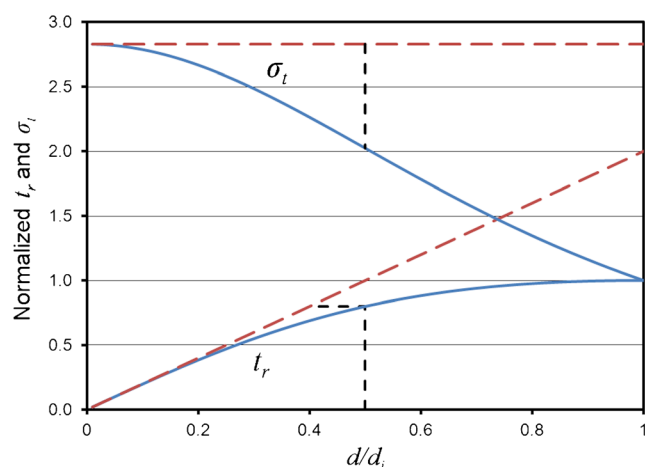


Fig. 5 Plots of steric-corrected t_r (blue full curve) and steric-uncorrected t_r (red dashed curve) normalized to the projected steric inversion time t_{ri} , and of steric-corrected σ_t (blue full curve) and steric-uncorrected σ_t (red dashed line) normalized to the projected σ_t at steric inversion

Under the same high retention conditions, the standard deviation in retention time σ_t can be obtained from Eq. (42) and the limiting forms of Eqs. (13) and (27):

$$\sigma_t = \left(\frac{2\lambda^4 w^2 t^0}{3(\alpha + \lambda)^3 D} \right)^{1/2} \quad (50)$$

Taking the same approach as for the retention ratio, and remembering that $D \propto 1/d$, it can be shown that

$$\frac{\sigma_t(d)}{\sigma_t(d_i)} = \left(\frac{2}{f^2 + 1} \right)^{3/2} \quad (51)$$

where $\sigma_t(d)$ is the standard deviation in retention time for a particle of diameter d , and $\sigma_t(d_i)$ is that for the projected inversion diameter d_i . If the steric correction is ignored, it can be shown that

$$\frac{\sigma_t'(d)}{\sigma_t'(d_i)} = \sqrt{8} \quad (52)$$

Equations (51) and (52) are also plotted in Fig. 5, labeled σ_t , as the full blue curve and dashed red line, respectively. The steric-corrected σ_t is seen to fall with increase of d , unlike the uncorrected σ_t' which remains constant. For d that is just half d_i , the uncorrected σ_t' is almost 40 % higher than the corrected σ_t . These differences are significant as it is not uncommon that such particle sizes are encountered in As-FIFFF analyses.

Conclusions

In As-FIFFF, the cross-channel component to fluid velocity varies with distance from the membrane-covered permeable accumulation wall and this leads to a departure from the ideal exponential concentration profile predicted for Sym-FIFFF where the cross-channel fluid velocity component is ideally constant. This in turn affects both the retention ratio and the nonequilibrium bandspreading parameter. The approach taken by Giddings and co-workers [1, 2] for the derivation of an equation for the nonequilibrium bandspreading parameter χ was modified to account for the variation in the cross-channel fluid velocity component. It was shown that as λ_0 decreases the retention ratio and the value of the function χ converge to those for Sym-FIFFF, as expected. It follows that under conditions of strong retention, we can expect As-FIFFF to fractionate samples as well as Sym-FIFFF, but for weaker retention, As-FIFFF will exhibit significantly higher bandspreading than Sym-FIFFF. It was mentioned that the non-uniform nature of the As-FIFFF system will lead to small deviations from the bandspreading predicted using the approach based on summation of contributions to variance for conditions at the

center of mass of a zone. This criticism does not apply to the equations describing local nonequilibrium plate height (Eqs. (20) and (36)).

The steric exclusion effect constitutes a first-order correction for finite particle size. The equations for both R and χ were derived with the inclusion of steric corrections. Other effects can also perturb elution, but these can often be minimized by optimizing carrier composition, reducing sample size, etc. The steric effect cannot be avoided, and it has been shown to be significant for particles much smaller than the projected inversion diameter. It is therefore important that it be taken into account when extracting quantitative information from experimental retention time measurements.

References

- Giddings JC (1968) Nonequilibrium theory of field-flow fractionation. *J Chem Phys* 49(1):81–85
- Giddings JC, Yoon YH, Caldwell KD, Myers MN, Hovingh ME (1975) Nonequilibrium plate height for field-flow fractionation in ideal parallel plate columns. *Sep Sci* 10(4):447–460
- Giddings JC (1966) A new separation concept based on a coupling of concentration and flow nonuniformities. *Sep Sci* 1(1):123–125
- Giddings JC, Myers MN (1978) Steric field-flow fractionation: a new method for separating 1 to 100 μm particles. *Sep Sci Technol* 13(8):637–645
- Giddings JC, Yang FJF, Myers MN (1974) Sedimentation field-flow fractionation. *Anal Chem* 46(13):1917–1924
- Kirkland JJ, Yau WW, Doerner WA, Grant JW (1980) Sedimentation field flow fractionation of macromolecules and colloids. *Anal Chem* 52(12):1944–1954
- Kirkland JJ, Rementer SW, Yau WW (1981) Time-delayed exponential field-programmed sedimentation field flow fractionation for particle-size-distribution analyses. *Anal Chem* 53(12):1730–1736
- Hovingh ME, Thompson GH, Giddings JC (1970) Column parameters in thermal field-flow fractionation. *Anal Chem* 42(2):195–203
- Runyon JR, Williams SKR (2011) A theory-based approach to thermal field-flow fractionation of polyacrylates. *J Chromatogr A* 1218(39):7016–7022
- Caldwell KD, Kesner LF, Myers MN, Giddings JC (1972) Electrical field-flow fractionation of proteins. *Science* 176(4032):296–298
- Somchue W, Siripinyanond A, Gale BK (2012) Electrical field-flow fractionation for metal nanoparticle characterization. *Anal Chem* 84(11):4993–4998
- Carpino F, Moore LR, Zborowski M, Chalmers JJ, Williams PS (2005) Analysis of magnetic nanoparticles using quadrupole magnetic field-flow fractionation. *J Magn Magn Mater* 293(1):546–552
- Williams PS, Carpino F, Zborowski M (2010) Characterization of magnetic nanoparticles using programmed quadrupole magnetic field-flow fractionation. *Philos Trans R Soc London, Ser A* 368(1927):4419–4437
- Giddings JC, Yang FJ, Myers MN (1976) Theoretical and experimental characterization of flow field-flow fractionation. *Anal Chem* 48(8):1126–1132
- Martin M, Hoyos M (2011) On the no-field method for void time determination in flow field-flow fractionation. *J Chromatogr A* 1218(27):4117–4125

16. Granger J, Dodds J, Leclerc D, Midoux N (1986) Flow and diffusion of particles in a channel with one porous wall: polarization chromatography. *Chem Eng Sci* 41(12):3119–3128
17. Wahlund K-G, Giddings JC (1987) Properties of an asymmetrical flow field-flow fractionation channel having one permeable wall. *Anal Chem* 59(9):1332–1339
18. Lee H-L, Reis JFG, Dohner J, Lightfoot EN (1974) Single-phase chromatography: solute retardation by ultrafiltration and electrophoresis. *AIChE J* 20(4):776–784
19. Doshi MR, Gill WN, Subramanian RS (1975) Unsteady reverse osmosis or ultrafiltration in a tube. *Chem Eng Sci* 30(12):1467–1476
20. Doshi MR, Gill WN (1979) Pressure field-flow fractionation or polarization chromatography. *Chem Eng Sci* 34(5):725–731
21. Jönsson JÅ, Carlshaf A (1989) Flow field flow fractionation in hollow cylindrical fibers. *Anal Chem* 61(1):11–18
22. Wijnhoven JEGJ, Koom J-P, Poppe H, Kok WT (1996) Influence of injected mass and ionic strength on retention of water-soluble polymers and proteins in hollow-fibre flow field-flow fractionation. *J Chromatogr A* 732(2):307–315
23. Litzén A, Wahlund K-G (1991) Zone broadening and dilution in rectangular and trapezoidal asymmetrical flow field-flow fractionation channels. *Anal Chem* 63(10):1001–1007
24. Williams PS (1997) Design of an asymmetrical flow field-flow fractionation channel for uniform channel flow velocity. *J Microcolumn Sep* 9(6):459–467
25. Giddings JC, Chen X, Wahlund K-G, Myers MN (1987) Fast particle separation by flow/steric field-flow fractionation. *Anal Chem* 59(15):1957–1962
26. Ratanathanawongs SK, Giddings JC (1992) Dual-field and flow-programmed lift hyperlayer field-flow fractionation. *Anal Chem* 64(1):6–15
27. Ahn JY, Kim KH, Lee JY, Williams PS, Moon MH (2010) Effect of asymmetrical flow field-flow fractionation channel geometry on separation efficiency. *J Chromatogr A* 1217(24):3876–3880
28. Williams PS, Giddings SB, Giddings JC (1986) Calculation of flow properties and end effects in field-flow fractionation channels by a conformal mapping procedure. *Anal Chem* 58(12):2397–2403
29. Goldman AJ, Cox RG, Brenner H (1967) Slow viscous motion of a sphere parallel to a plane wall—II. Couette flow *Chem Eng Sci* 22(4):653–660
30. Williams PS, Koch T, Giddings JC (1992) Characterization of near-wall hydrodynamic lift forces using sedimentation field-flow fractionation. *Chem Eng Commun* 111:121–147
31. Pasol L, Martin M, Ekiel-Jeżewska ML, Wajnryb E, BŁawdziewicz J, Feuillebois F (2011) Motion of a sphere parallel to plane walls in a Poiseuille flow. Application to field-flow fractionation and hydrodynamic chromatography. *Chem Eng Sci* 66(18):4078–4089
32. Giddings JC (1978) Displacement and dispersion of particles of finite size in flow channels with lateral forces. Field-flow fractionation and hydrodynamic chromatography. *Sep Sci Technol* 13(3):241–254
33. Giddings JC (1979) ERRATA. Displacement and dispersion of particles of finite size in flow channels with lateral forces. Field-flow fractionation and hydrodynamic chromatography. *Sep Sci Technol* 14(9):869–870
34. Beavers GS, Joseph DD (1967) Boundary conditions at a naturally permeable wall. *J Fluid Mech* 30(1):197–207
35. Davis JM (1991) Influence of crossflow hydrodynamics on retention ratio in flow field-flow fractionation. *Anal Chim Acta* 246(1):161–169
36. Granger J, Dodds J, Midoux N (1989) Laminar flow in channels with porous walls. *Chem Eng J* 42(3):193–204
37. Williams PS, Giddings JC (1994) Theory of field-programmed field-flow fractionation with corrections for steric effects. *Anal Chem* 66(23):4215–4228
38. Giddings JC (1963) Plate height of nonuniform chromatographic columns. Gas compression effects, coupled columns, and analogous systems. *Anal Chem* 35(3):353–356
39. Giddings JC, Williams PS, Beckett R (1987) Fractionating power in programmed field-flow fractionation: exponential sedimentation field decay. *Anal Chem* 59(1):28–37
40. Williams PS, Giddings JC, Beckett R (1987) Fractionating power in sedimentation field-flow fractionation with linear and parabolic field decay programming. *J Liq Chromatogr* 10(8–9):1961–1998
41. Williams PS, Giddings JC (1987) Power programmed field-flow fractionation: a new program form for improved uniformity of fractionating power. *Anal Chem* 59(17):2038–2044
42. Williams PS, Kellner L, Beckett R, Giddings JC (1988) Comparison of experimental and theoretical fractionating power for exponential field decay sedimentation field-flow fractionation. *Analyst* 113(8):1253–1259
43. Williams PS, Giddings MC, Giddings JC (2001) A data analysis algorithm for programmed field-flow fractionation. *Anal Chem* 73(17):4202–4211
44. Blumberg LM, Berger TA (1992) Variance of a zone migrating in a non-uniform time-invariant linear medium. *J Chromatogr* 596(1):1–13
45. Caldwell KD, Nguyen TT, Myers MN, Giddings JC (1979) Observations on anomalous retention in steric field-flow fractionation. *Sep Sci Technol* 14(10):935–946
46. Myers MN, Giddings JC (1982) Properties of the transition from normal to steric field-flow fractionation. *Anal Chem* 54(13):2284–2289
47. Shendruk TN, Tahvildari R, Catafard NM, Andrzejewski L, Gigault C, Todd A, Gagne-Dumais L, Slater GW, Godin M (2013) Field-flow fractionation and hydrodynamic chromatography on a microfluidic chip. *Anal Chem* 85(12):5981–5988
48. Williams PS, Xu Y, Reschiglian P, Giddings JC (1997) Colloid characterization by sedimentation field-flow fractionation: correction for particle-wall interaction. *Anal Chem* 69(3):349–360
49. Du Q, Schimpf ME (2002) Correction for particle-wall interactions in the separation of colloids by flow field-flow fractionation. *Anal Chem* 74(11):2478–2485
50. Beckett R, Giddings JC (1997) Entropic contribution to the retention of nonspherical particles in field-flow fractionation. *J Colloid Interface Sci* 186(1):53–59
51. Phelan FR Jr, Bauer BJ (2007) Simulation of nanotube separation in field-flow fractionation (FFF). *Chem Eng Sci* 62(17):4620–4635
52. Phelan FR Jr, Bauer BJ (2009) Comparison of steric effects in the modeling of spheres and rodlike particles in field-flow fractionation. *Chem Eng Sci* 64(8):1747–1758
53. Gigault J, Cho TJ, MacCuspie RI, Hackley VA (2013) Gold nanorod separation and characterization by asymmetric-flow field flow fractionation with UV-Vis detection. *Anal Bioanal Chem* 405(4):1191–1202